

# SCIENTIFIC REPORTS

OPEN

## Tuning magnetic properties for domain wall pinning via localized metal diffusion

T. L. Jin<sup>1,2</sup>, M. Ranjbar<sup>1</sup>, S. K. He<sup>2</sup>, W. C. Law<sup>1</sup>, T. J. Zhou<sup>2</sup>, W. S. Lew<sup>1</sup>, X. X. Liu<sup>3</sup> & S. N. Piramanayagam<sup>1</sup>

Precise control of domain wall displacement in nanowires is essential for application in domain wall based memory and logic devices. Currently, domain walls are pinned by creating topographical notches fabricated by lithography. In this paper, we propose localized diffusion of non-magnetic metal into ferromagnetic nanowires by annealing induced mixing as a non-topographical approach to form pinning sites. As a first step to prove this new approach, magnetodynamic properties of permalloy ( $\text{Ni}_{80}\text{Fe}_{20}$ ) films coated with different capping layers such as Ta, Cr, Cu and Ru were investigated. Ferromagnetic resonance (FMR), and anisotropy magnetoresistance (AMR) measurements were carried out after annealing the samples at different temperatures ( $T_{an}$ ). The saturation magnetization of  $\text{Ni}_{80}\text{Fe}_{20}$  film decreased, and damping constant increased with  $T_{an}$ . X-Ray photoelectron spectroscopy results confirmed increased diffusion of Cr into the middle of  $\text{Ni}_{80}\text{Fe}_{20}$  layers with  $T_{an}$ . The resistance vs magnetic field measurements on nanowires showed intriguing results.

Domain wall based devices such as racetrack memory have been proposed as promising candidates for high-density, non-volatile information storage with a low energy consumption<sup>1–9</sup>. Such devices are also considered as 3-terminal memory devices at a higher level of memory-storage hierarchy. Information in these devices are stored in the directions of domain magnetization and read and written by moving domain walls. Since the domain wall motion is based on spintronics principles, the reading and writing process do not require mechanical rotation as in hard disk drives<sup>8–10</sup>. Figure 1(a) shows the simplified schematic diagram of domain wall memory that stores information in nanowire based on domain orientation and domain wall movement by pulse current for reading (writing) information. Domain wall motion along the nanowire, driven by in-plane current, has been investigated tremendously<sup>9,11–13</sup>. The theory for spin-transfer torque was reported by Berger and Slonczewski in 1996. Independently, they pointed out that a spin polarized current is generated when an electric current that goes through the ferromagnetic layer transfers the spin angular momentum to local magnetic moment via electron exchange interaction. This exerts a torque on the local magnetization, resulting in domain wall motion<sup>14–18</sup>. In earlier research work, the torque exerted by in-plane current named as spin transfer torque (STT), drove domain wall motion in the opposite direction of electric current flow, and is often considered as an effective field<sup>19,20</sup>. In those cases, the velocity of domain wall was just 100 m/s<sup>19,20</sup>. In the recent years, faster domain wall motion up to 400 m/s, has been observed in perpendicular magnetic anisotropy (PMA) material using pure spin polarized current<sup>12,21,22</sup>. In such structures, the pure spin polarized current originates from the electric current in heavy metal due to strong spin orbit coupling and Rashba effect, which is named as spin orbit torque (SOT)<sup>23,24</sup>. The high speed of domain wall motion also relate to the chiral domain wall structure in PMA material that is formed by interfacial Dzyaloshinskii-Doriya interaction (DMI)<sup>25</sup>. Recently, the speed of domain wall 750 m/s was reported in synthetic anti-ferromagnetic structure driven by SOT<sup>26</sup>.

Spin polarized current gives a high speed performance of domain wall devices. However, for reliable operation of domain wall devices, the other key issue is the control of domain wall motion by pinning domain walls uniformly<sup>9,27–29</sup>. In the absence of pinning sites, the domain walls may be swept rapidly without precise control. In general cases, the pinning sites for domain wall devices are fabricated by complicated lithography process, like

<sup>1</sup>Division of Physics and Applied Physics, School of Physical and Mathematical Sciences, Nanyang Technological University, Singapore, 637371, Singapore. <sup>2</sup>Data Storage Institute, A\*STAR (Agency for Science, Technology and Research), 2 Fusionopolis Way, #08-01 Innovis, Singapore, 138634, Singapore. <sup>3</sup>Department of Electrical and Computer Engineering, Shinshu University, Wakasato 4-17-1, Nagano, 380-8553, Japan. Correspondence and requests for materials should be addressed to S.N.P. (email: [prem@ntu.edu.sg](mailto:prem@ntu.edu.sg))

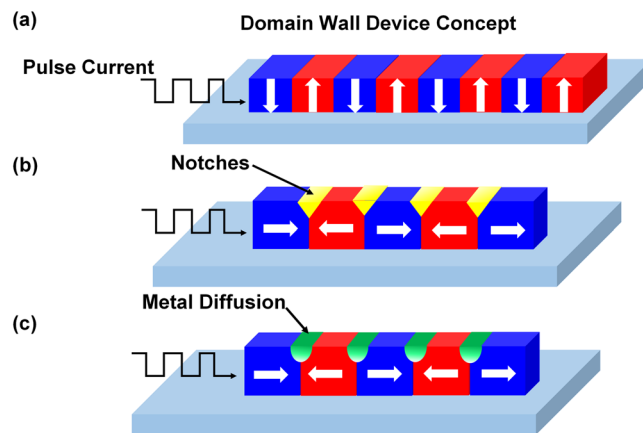


**Figure 1.** Illustration of domain wall device concept and the control of domain wall propagation using different structures. (a) Information stored in nanowire based on domain orientation and an illustration of domain wall movement by pulse current for reading (writing) information. (b) Illustration of controlling domain wall propagation using notches. (c) Schematic representation of the proposed method to control domain wall motion using metal diffusion.

creation of notches and zigzag patterns in the ferromagnetic nanowire<sup>6,29–31</sup>. Moreover, the pinning effect could be non-uniform due to the shape and size variations, as shown in Fig. 1(b). Tuning the properties of nanowire locally to pin domain wall at precise position is more efficient for domain wall devices. Exchange bias has been proposed as one such method<sup>32</sup>. Several other methods to tune the properties of ferromagnetic, like focused Ga<sup>+</sup> ion irradiation on film, non-magnetic metal doped in ferromagnetic film by ion implantation or co-deposition have also been reported<sup>33–37</sup>. Here, we propose an alternative method for controlling domain wall displacement by tuning the composition of ferromagnetic material locally with annealing to stabilize domain walls, as shown in Fig. 1(c). Experimental investigations were carried out to understand the effect of composition on the properties of Ni<sub>80</sub>Fe<sub>20</sub> film. Diffusion of various metals including Ta, Cr, Cu and Ru, which are widely used in memory industry, was achieved at the interface through annealing under certain temperature. The Ni<sub>80</sub>Fe<sub>20</sub> devices with cross pinning sites have been fabricated to show that this method could be useful in domain wall pinning.

## Experiments

In order to find out if composition in magnetic films can be controlled by annealing induced mixing and if the properties can be tailored, 10 nm thick Ni<sub>80</sub>Fe<sub>20</sub> thin films were sputtered with different metallic capping layers. The film stacks of the type Si/(SiO<sub>2</sub>)/Ni<sub>80</sub>Fe<sub>20</sub> (10 nm)/X (5 nm), were deposited by dc magnetron sputtering. Here, X refers to the capping metallic layers such Ta, Cr, Cu and Ru. Permalloy film without capping layer was also prepared as reference. After deposition, Ni<sub>80</sub>Fe<sub>20</sub> films with capping layer were annealed for 1 hour at different annealing temperatures,  $T_{an}$ , from 100 °C to 400 °C in vacuum. Alternating Gradient Force Magnetometer (AGFM), and broadband Ferromagnetic resonance (FMR) spectroscopy measurements were used to obtain the magnetic properties at different  $T_{an}$ .

## Results and Discussion

Normalized magnetic hysteresis loops (M-H) of pure Ni<sub>80</sub>Fe<sub>20</sub> (NiFe) thin film, measured along in plane (IP) and out of plane (OOP) directions, are shown in Fig. 2(a). The M-H loop shows well defined in-plane anisotropy of Ni<sub>80</sub>Fe<sub>20</sub> film, with a low coercivity of about 15 Oe. In order to study quantitatively the magnetodynamics properties of films, broadband ferromagnetic resonance (FMR) measurements were carried out at room temperature. Figure 2(b–d) shows various steps of FMR linewidth measurements for pure Ni<sub>80</sub>Fe<sub>20</sub> film, supporting the quality of the film and the measurement. The saturation magnetization is  $726 \pm 2$  emu/cc. The Gilbert damping constant is small for Ni<sub>80</sub>Fe<sub>20</sub> film, about  $0.0077 \pm 2 \times 10^{-4}$ , and is consistent with the values reported in literature<sup>38,39</sup>.

Standard properties shown in Fig. 2, verified the quality of the prepared permalloy films. As a next step, the static and dynamic properties of Ni<sub>80</sub>Fe<sub>20</sub> film samples without capping and with different metallic capping layers annealed at different  $T_{an}$  from 100 °C to 400 °C were studied by measuring normalized M-H loops and FMR spectral signal. The FMR spectral signal was obtained by sweeping the magnetic field, which is parallel to film direction, with varying frequency from 2 GHz to 25 GHz. In this configuration, the resonance frequency and applied field follow the Kittel equation relation and the half linewidth of the resonances peak was also measured as a function of frequency. Figures 3(a) and (b) show the resonance frequency vs applied field and the half linewidth vs resonance frequency of Ni<sub>80</sub>Fe<sub>20</sub> film without capping layer annealed at different  $T_{an}$ . To extract the saturation magnetization ( $M_s$ ) of Ni<sub>80</sub>Fe<sub>20</sub> film samples after annealing, the Kittel equation was fitted to the data as shown in Fig. 3(a).  $M_s$  did not show much change after annealing. Even at higher  $T_{an} = 400$  °C, the value of  $M_s$  was maintained at  $723 \pm 3$  emu/cc. But the damping constant, obtained by fitting the linewidth with resonance frequency in Fig. 3(b) (Refer to the Method part), increased after annealing, going up to  $0.0122 \pm 2 \times 10^{-4}$  at  $T_{an} = 400$  °C<sup>39,40</sup>. The increase in damping is probably due to the diffusion of oxygen into NiFe from substrate Si (SiO<sub>2</sub>) arising from an increase in the magnon scattering<sup>41</sup>. The damping constant showed a remarkably high value of  $0.0185 \pm 3 \times 10^{-4}$  at  $T_{an} = 500$  °C. It is well known that the depinning field increases with the damping

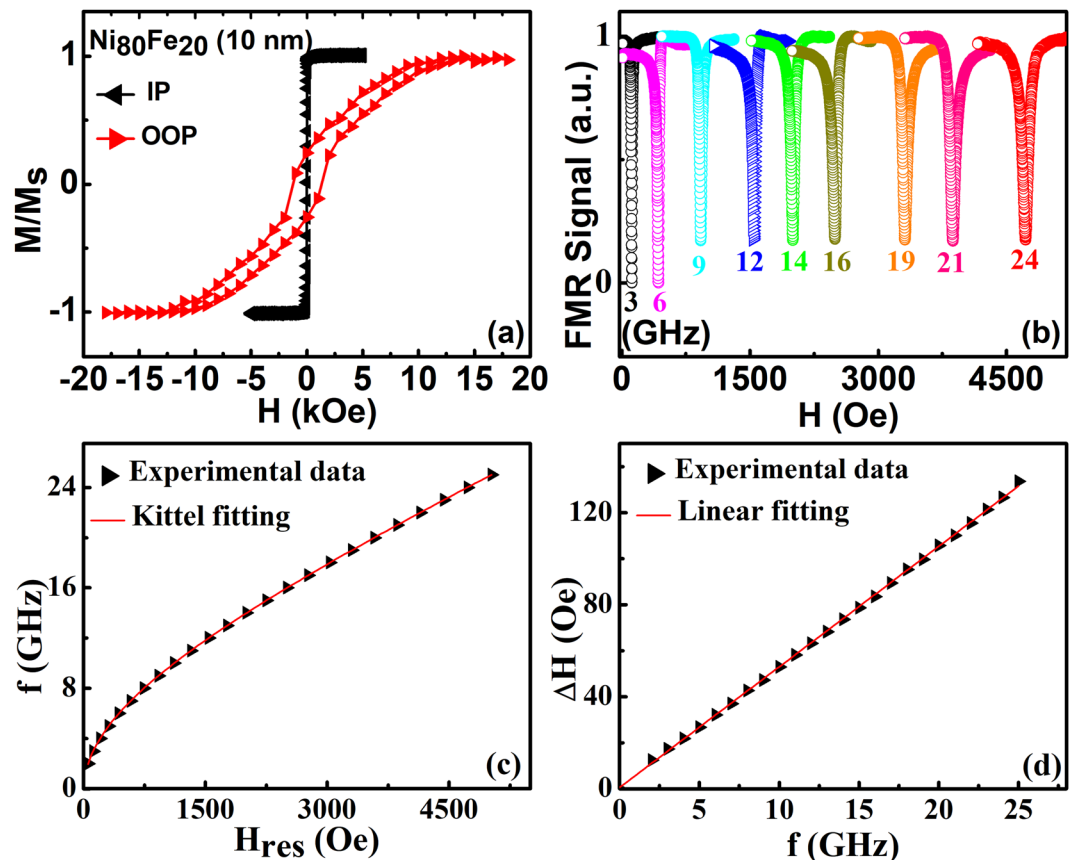


**Figure 2.** (a) The normalized hysteresis loops of  $\text{Ni}_{80}\text{Fe}_{20}$  along in plane (IP) direction and out of plane (OOP) directions. (b) The FMR signal for  $\text{Ni}_{80}\text{Fe}_{20}$  thin film with thickness of 10 nm with magnetic field applied parallel to sample plane. (c) Resonance frequency as a function of resonance field and (d) FMR linewidths as a function of resonance frequency.

constant<sup>42</sup>. As a result, a higher current is required to drive domain wall motion, which is not desired. Therefore, in the subsequent experiments, we fixed the maximum annealing temperature to be 400 °C.

The magnetic properties of NiFe with different capping layer, annealed at different temperatures, are shown in Fig. 3(c) to (f). Saturation magnetization ( $M_s$ ) decreases with increasing  $T_{an}$  from 100 °C to 400 °C for all metallic capping layer as shown in Fig. 3(c). The decrease has been the most significant in the case of Cr, where the effective magnetization  $M_s$  drops down to  $350 \pm 8$  emu/cc at 400 °C. In the case of Cu capping layer,  $M_s$  decreases from  $720 \pm 3$  emu/cc to  $624 \pm 5$  emu/cc with increasing  $T_{an}$  to 400 °C, while for Ta and Ru, magnetization decreases at a much slower rate. We also found beyond 200 °C, saturation field along the perpendicular direction increases steadily with  $T_{an}$ . Figure 3(d–f) show the magnetodynamic properties of  $\text{Ni}_{80}\text{Fe}_{20}/X$  such as Gyromagnetic ratio (d), damping constant (e) and inhomogeneous broadening (f) at different  $T_{an}$ . The Gyromagnetic ratio ( $\gamma/2\pi$ ) remained at about 2.96 MHz/Oe for most all the samples. For Cu and Cr capping layer, it increases to 3.01 and 3.04 (MHz/Oe) at  $T_{an} = 400$  °C respectively. The damping constant of  $\text{Ni}_{80}\text{Fe}_{20}$  increased with  $T_{an}$  for all capping layers<sup>33,35,36</sup>. Among all the elements investigated, Cr showed the strongest effect and Ta capping layer had the least effect. The damping constant of  $\text{Ni}_{80}\text{Fe}_{20}$  is not influenced much for  $T_{an} < 300$  °C. However, for Cr, an increase in  $\alpha$  by 246% at  $T_{an} = 400$  °C was observed. For Cu capping layer, the damping constant of the annealed films increased to  $0.01198 \pm 3 \times 10^{-5}$  at  $T_{an} = 400$  °C<sup>43</sup>. The inhomogeneous broadening value is small for all capping layers at room temperature, and it shows the increasing trend for Cr and Cu capping layers, increasing to 66 Oe and 28 Oe respectively with  $T_{an}$ . However, it does not show much change for Ta and Ru capping layers. Anisotropy field was very small as expected for all  $\text{Ni}_{80}\text{Fe}_{20}/X$  films and it did not show significant changes after annealing.

The investigations discussed so far indicate that the metal diffusion causes changes in the properties of  $\text{Ni}_{80}\text{Fe}_{20}$  film and among several elements, Cr has the strongest effect both in static ( $M_s$ ) and dynamic properties ( $\alpha$ ). It is worthwhile to compare the properties with those reported in literature<sup>35,43–46</sup>. Ruiz-Calaforra *et al.*, have studied the effect of metal capping layers adjacent to NiFe layer. Some of their samples (9–11 nm thickness of NiFe) are similar to our samples at room temperature. In their samples, the presence of a Pt layer enhances the damping constant significantly due to spin pumping. In comparison, Ru enhances the damping constant to a larger extent than Cr. A similar trend in this study was also observed at room temperature. However, absolute values and the changes in the damping constant are smaller in our samples due to less noise in our FMR data and probably the nature of deposition process of our samples. In our samples, Cr capping layers did not cause a significant change in the damping constant at room temperature. However, it causes a large increase in damping constant after

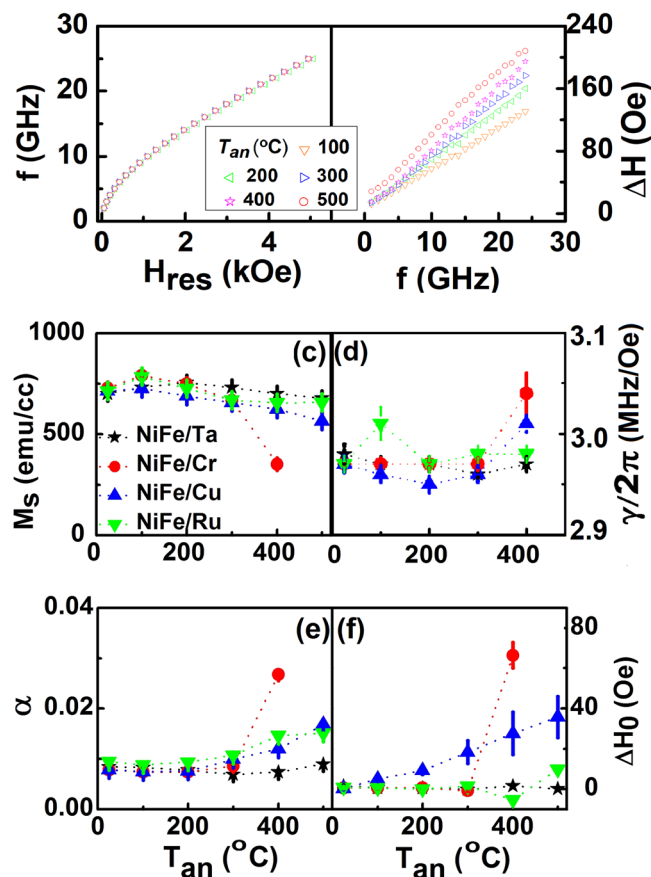


**Figure 3.**  $\text{Ni}_{80}\text{Fe}_{20}$  without capping layer at different annealing temperatures ( $T_{an}$ ), resonance frequency as a function of resonance field (a) and FMR half linewidths as a function of resonance frequency (b). Magnetic properties of  $\text{Ni}_{80}\text{Fe}_{20}/\text{X}$  ( $\text{NiFe}/\text{X} = \text{Ta}, \text{Cr}, \text{Cu}, \text{Ru}$ ) at different annealing temperatures ( $T_{an}$ ). The effective saturation magnetization (c), Gyromagnetic ratio (d), damping constant (e) and inhomogeneous broadening (f).

annealing. From this comparison, the increase in damping constant is mainly attributed to the annealing induced mixing. Faulkner *et al.*<sup>36</sup> have studied the influence of Cr doping by ion implantation in NiFe. They too observe a similar increase in damping constant, a decrease in  $M_s$  and anisotropy energy ( $K_u$ ). It is well known that the addition of Cr causes decrease of magnetization in ferromagnetic systems. Cr spins are believed to couple antiferromagnetically to the spins of host atoms and as a result, our samples too show a decrease of  $M_s$ .

In order to understand the diffusion of Cr in  $\text{Ni}_{80}\text{Fe}_{20}$  film further, X-ray photoelectron spectroscopy (XPS) was carried out. Figure 4(a) to (e) show the Cr diffusion effect with the different  $T_{an}$ . It can be seen that the Cr diffusion is less for  $T_{an}$  below 300 °C, but shoots up for  $T_{an}$  above 300 °C. Figure 4(f) summarizes the concentration of Cr, closer to the bottom of  $\text{Ni}_{80}\text{Fe}_{20}$  layer (7 minutes sputter etching time), for different  $T_{an}$ . The changes in saturation magnetization  $M_s$ , damping constant and the other properties can be explained to be arising as a result of Cr diffusion, which is significantly stronger at higher temperatures.

In order to understand if the elements diffuse in to NiFe uniformly and form solid solutions or if they form clusters, we also carried out elemental analysis of the interfaces. For this purpose, energy dispersive X-ray spectroscopy was carried out by using Transmission Electron Microscopy (TEM) equipment. Figure 5 shows the TEM cross section configuration of NiFe with Cr capping layer annealed at 400 °C and Energy Dispersive X-ray (EDX) Spectroscopy analysis images. The results indicate that the diffusion of Cr into NiFe layer by annealing is uniform and hence a solid solution. Different elements may behave differently and their behavior may, to some extent, be predicted from the phase diagrams<sup>47–49</sup>. It is well known that Cu does not mix well with Fe and hence, we should see different results. Figure 6 shows the EDX analysis of elemental concentration of Si (substrate), Ni, Fe and Cu. It can be seen that the copper atoms do not diffuse so uniformly like Cr atoms.

In order to prove that the local modification is effective in stabilizing the domain walls, NiFe magnetic wires with 1  $\mu\text{m}$  wide and 100  $\mu\text{m}$  long were fabricated by Electron-beam lithography (EBL) and argon ion milling. A Ta seedlayer was used to prevent the diffusion of oxygen from Si substrate and to improve the adhesion<sup>50</sup>. After the NiFe wires were fabricated, Cr cross lines were fabricated by EBL, followed by 5 nm thick Cr deposition. The NiFe magnetic wire was annealed in vacuum chamber at 400 °C atmosphere before all the electrode fabrication. A top view micrograph of the magnetic wire is shown in Fig. 7(b). The inset in Fig. 7(b) is the line-scan of Atomic Force Microscopy (AFM) images of the NiFe wire with Cr wires, and the height profile shows that the Cr is on top

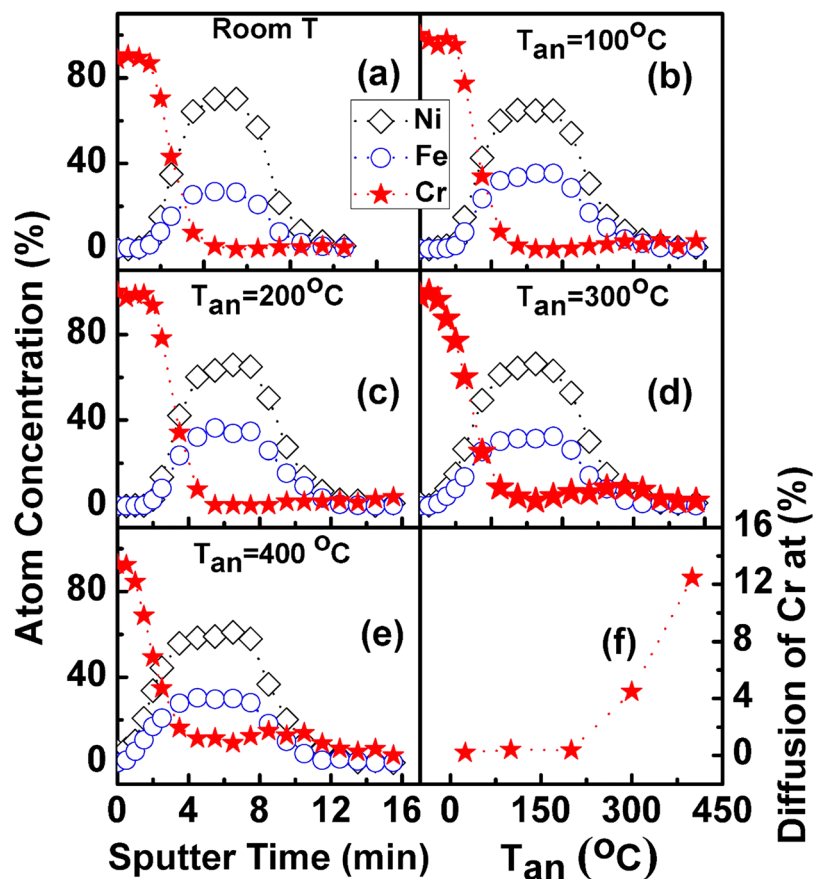


**Figure 4.** XPS analysis for Cr diffusion effect vs the  $T_{an}$  from 100 °C to 400 °C ((a) to (e)) and (f) summarizes the concentration of Cr diffusion into  $Ni_{80}Fe_{20}$  layer with the  $T_{an}$  taking the diffusion value of Cr at 7 minutes sputter etching time.

of the NiFe wire. The NiFe magnetic wire without Cr pinning cross lines also was prepared as reference sample using EBL, as shown in Fig. 7(a).

NiFe without Cr magnetic wire shows typical properties in AMR measurements. When field was applied parallel to the current direction, a high resistance was observed and for field perpendicular to the current direction, a drop in resistance was observed at high fields as shown in Fig. 7(c). A high magnetic field perpendicular to the nanowire orients the magnetization in perpendicular direction to the current and hence such a drop is observed. In the case of magnetic field along the nanowire direction, the change in resistance is not significant, as the domains are swept rapidly and hence the magnetization is always parallel or antiparallel to the current direction.

In the case of NiFe wires with Cr pinning bars, the results for the case of current perpendicular to the field are similar. However, the observed results for the case of current parallel to the magnetic field are different and interesting. Two obvious dips are observed in the R-H curves as shown as Fig. 7(d). These dips were observed at fields, as high as  $-100$  Oe, which are much larger than the coercivity. Although such a dip could arise as a result of domain wall pinning, the significantly large magnitude of the dip warrants further investigation to understand the origin of such a dip. When a large magnetic field (600 Oe) along the nanowire was applied, the magnetization is saturated and parallel to the current, and the resistance was larger again.

## Conclusion

To summarize, a novel domain wall pinning method using compositional modifications is proposed and the materials level investigations are carried out experimentally in detail. Investigations at thin-film level indicate that the diffusion caused by annealing is useful to form domain wall pinning sites. Diffusion of Cr proves to be more effective in comparison to other elements such as Ta, Cu and Ru in changing the magnetic and magneto-dynamic properties. Domain wall devices were fabricated and investigated using resistance measurements as a gauge of domain wall pinning. Compared to permalloy wires without Cr-diffused pinning sites, permalloy wires with Cr-diffused pinning sites exhibited different properties. Although annealing is investigated in this study, compositional modification can also be carried out using techniques such as ion-implantation. For much higher density operation, materials with a perpendicular magnetic anisotropy may be used, although this study only uses permalloy<sup>29,50</sup>. The method proposed in this study is promising to stabilize and control domain wall propagation in domain wall memory devices.

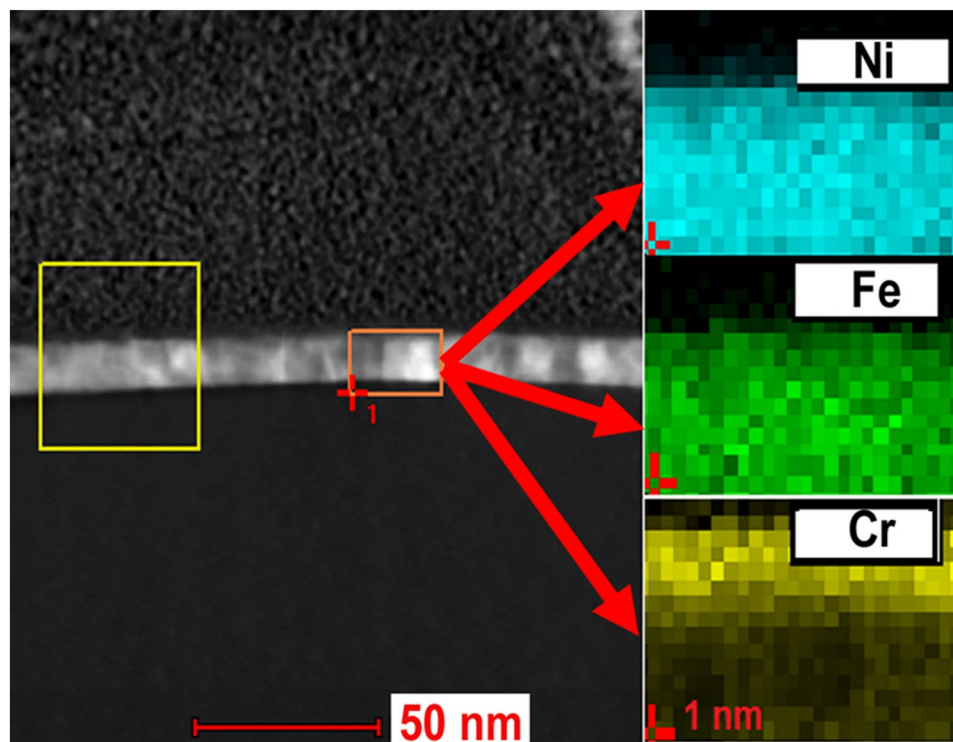


**Figure 5.** TEM cross configuration and the EDX analysis pattern result at the square area shown as the arrow. From top to bottom, the images show the Ni, Fe and Cr the quantitative analysis.

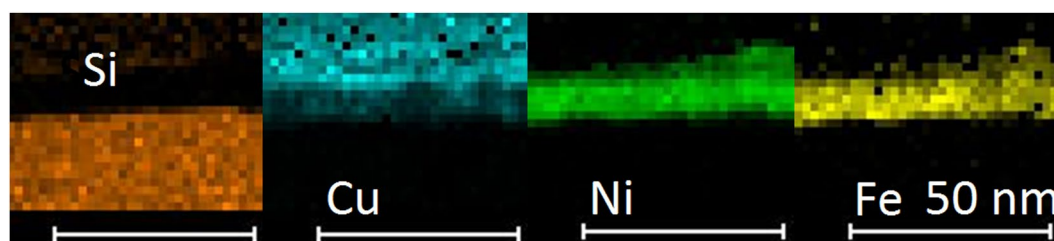


**Figure 6.** Elemental map of Si, Cu, Ni and Fe in Si substrate/NiFe/Cu structures.

## Methods

**Sample fabrication.** All the  $\text{Ni}_{80}\text{Fe}_{20}$  samples were deposited on silicon substrates covered by  $500\ \mu\text{m}$  thermal  $\text{SiO}_2$  layer via DC magnetron sputtering in AJA sputtering system at room temperature. The base pressure of the main chamber was superior to  $1.1 \times 10^{-7}$  Torr. The argon gas pressure for  $\text{Ni}_{80}\text{Fe}_{20}$  layer was fixed at 2 mTorr and the deposition rate was  $0.12\ \text{nm s}^{-1}$  fired at the DC power of 40 W. Different capping layers Ta, Cr, Cu, and Ru were deposited at an argon pressure of 3 mTorr respectively. 10 nm thick  $\text{Ni}_{80}\text{Fe}_{20}$  thin film with different non-magnetic metal capping layers ( $\text{Ni}_{80}\text{Fe}_{20}/\text{X} = \text{Ta}, \text{Cr}, \text{Cu}, \text{and Ru}$ ) of 5 nm samples were fabricated. After deposition,  $\text{Ni}_{80}\text{Fe}_{20}$  films with capping layer were annealed for 1 hour at different  $T_{\text{an}}$  from  $100\ ^\circ\text{C}$  to  $400\ ^\circ\text{C}$  in vacuum condition with base pressure below  $5 \times 10^{-7}$  Torr.

Thickness calibration is based on measuring the thickness of the stepped film by using Atomic Force Microscopy. The stepped film was fabricated by drawing straight line using a marker pen, followed by washing off in Isopropyl alcohol.

The fabrication of NiFe and Cr wires was made by E-beam lithography (EBL). The first layer of resist over NiFe wire was exposed under 20 kV voltage and  $7\ \mu\text{m}$  aperture. After exposure, Ar ion-milling was done to eliminate the unwanted film. The second layer of resist over NiFe wires was exposed under 10 kV voltage and  $30\ \mu\text{m}$  aperture. After developing, Cr was deposited in the holes of the second layer of resist. The device in vacuum chamber was annealed at  $400\ ^\circ\text{C}$  for one hour to make Cr diffusion into the NiFe wire at the cross section to form pinning sites. After this, fabrication of the electrode pad was carried out by exposing the resist under 20 kV and  $120\ \mu\text{m}$  aperture.

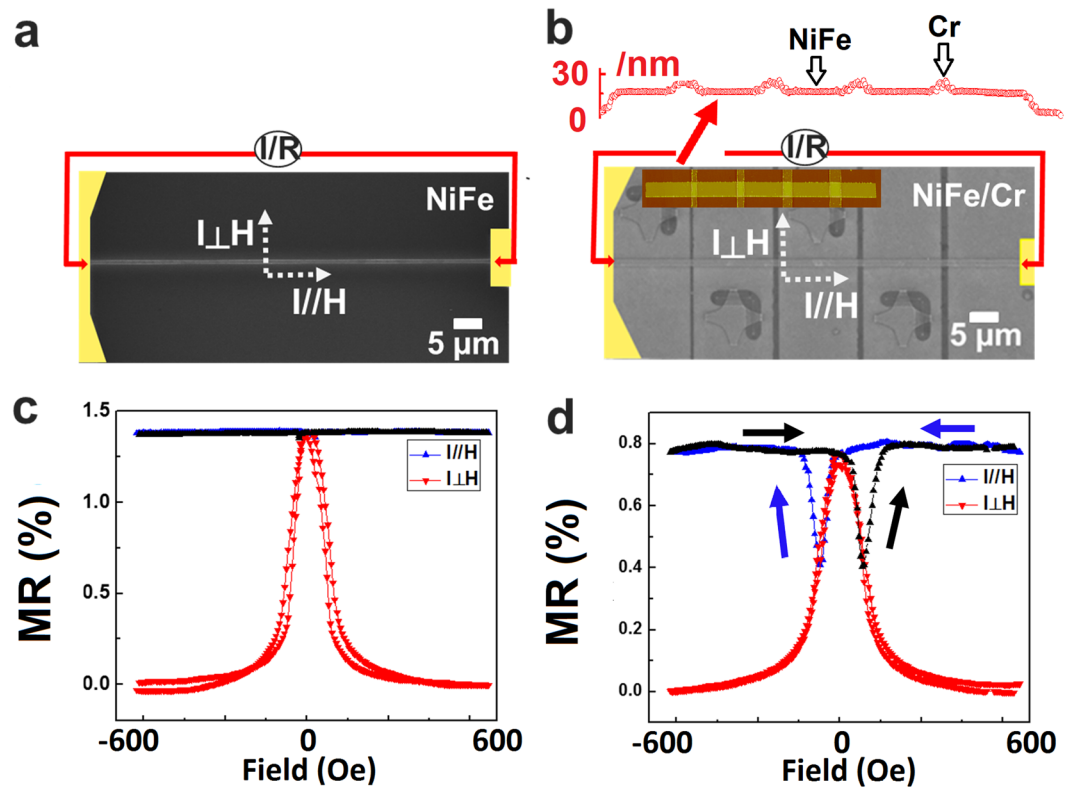


**Figure 7.** Schematic representation of NiFe magnetic wire without Cr pinning cross site (a) and with Cr pinning sites (b). The insert figure is AFM image of NiFe wire with Cr cross wires. The resistance ratio of NiFe with Cr pinning bars (c) and without Cr pinning sites (d) measured by applying in-plane magnetic field along and perpendicular to NiFe wire direction.

**Sample Characterization.** Normalized magnetic hysteresis loops (M-H) of  $\text{Ni}_{80}\text{Fe}_{20}$  thin film along in plane (IP) and out of plane (OOP) directions were carried out at room temperature with the magnetic sweeping from  $-20$  kOe to 20 kOe. Broadband ferromagnetic resonance (FMR) measurements were carried out using a Keysight PNA N5222A vector network analyzer with a  $117 \mu\text{m}$  width coplanar waveguide at room temperature to study quantitatively the magnetic static and dynamics properties of films, including saturation magnetization ( $M_s$ ), in-plane anisotropy field ( $H_k$ ), Gyromagnetic ratio ( $\gamma$ ), damping constant ( $\alpha$ ) and inhomogeneous broadening ( $\Delta H_0$ ). The microwave frequency was varied from 2 GHz to 25 GHz and the magnetic field was applied parallel to sample plane. The ferromagnetic resonance frequency  $f$ , in the applied field is determined by the following equation:

$$f = \frac{\gamma}{2\pi} \left[ (H_{\text{appl}} + H_k) \times (H_{\text{appl}} + H_k + M_s) \right]^{\frac{1}{2}} \quad (1)$$

The damping relation with frequency dependent FMR linewidths:

$$\Delta H = \frac{4\pi}{\gamma} \alpha f + \Delta H_0. \quad (2)$$

## References

1. Parkin, S. *et al.* Magnetically engineered spintronic sensors and memory. *Proceedings of the IEEE* **91**, 661–680 (2003).
2. Allwood, D. A. *et al.* Magnetic domain-wall logic. *Science* **309**, 1688–1692 (2005).
3. Chappert, C., Fert, A. & Van Dau, F. N. The emergence of spin electronics in data storage. *Nat. Mater.* **6**, 813–823 (2007).
4. Sbiaa, R. & Piramanayagam, S. N. Multi-level domain wall memory in constricted magnetic nanowires. *Applied Physics A-Materials Science & Processing* **114**, 1347–1351 (2014).
5. Dong, Q. *et al.* In 2015 IEEE International Symposium on Circuits and Systems IEEE International Symposium on Circuits and Systems 585–588 (2015).
6. Parkin, S. & Yang, S. H. Memory on the racetrack. *Nat. Nanotechnol.* **10**, 195–198 (2015).
7. Vandermeulen, J., V de Wiele, B., Dupre, L. & Van Waeyenberge, B. Logic and memory concepts for all-magnetic computing based on transverse domain walls. *J. Phys. D-Appl. Phys.* **48**, 275003 (2015).
8. Hayashi, M., Thomas, L., Moriya, R., Rettner, C. & Parkin, S. S. P. Current-controlled magnetic domain-wall nanowire shift register. *Science* **320**, 209–211 (2008).
9. Parkin, S. S. P., Hayashi, M. & Thomas, L. Magnetic domain-wall racetrack memory. *Science* **320**, 190–194 (2008).
10. Annunziata, A. J. *et al.* Racetrack Memory Cell Array with Integrated Magnetic Tunnel Junction Readout. 2011 IEEE International Electron Devices Meeting (IEDM) (2011).

11. Ueda, K. *et al.* Current-induced domain wall motion in Co/Ni nano-wires with different Co and Ni thicknesses. *Journal of Physics: Conference Series* **266**, 012110 (2011).
12. Koyama, T. *et al.* Observation of the intrinsic pinning of a magnetic domain wall in a ferromagnetic nanowire. *Nat. Mater.* **10**, 194–197 (2011).
13. Kim, K.-J. *et al.* Observation of magnetic domain-wall dynamics transition in Co/Ni multilayered nanowires. *Appl. Phys. Lett.* **101**, 022407 (2012).
14. Slonczewski, J. C. Current-driven excitation of magnetic multilayers. *J. Magn. Magn. Mater.* **159**, L1–L7 (1996).
15. Zhang, S., Levy, P. M. & Fert, A. Mechanisms of spin-polarized current-driven magnetization switching. *Phys. Rev. Lett.* **88**, 236601 (2002).
16. Ji, Y., Chien, C. L. & Stiles, M. D. Current-induced spin-wave excitations in a single ferromagnetic layer. *Phys. Rev. Lett.* **90**, 106601 (2003).
17. Li, Z. & Zhang, S. Magnetization dynamics with a spin-transfer torque. *Phys. Rev. B* **68**, 024404 (2003).
18. Kasai, S., Nakatani, Y., Kobayashi, K., Kohno, H. & Ono, T. Current-driven resonant excitation of magnetic vortices. *Phys. Rev. Lett.* **97**, 107204 (2006).
19. Seo, S. M., Kim, K. W., Ryu, J., Lee, H. W. & Lee, K. J. Current-induced motion of a transverse magnetic domain wall in the presence of spin Hall effect. *Appl. Phys. Lett.* **101**, 022405 (2012).
20. Yamanouchi, M., Chiba, D., Matsukura, F. & Ohno, H. Current-induced domain-wall switching in a ferromagnetic semiconductor structure. *Nature* **428**, 539–542 (2004).
21. Ohshima, N. *et al.* Real space observation of current-induced magnetic domain wall displacement in Co/Ni nano-wire by photoemission electron microscopy. *Journal of physics. Condensed matter: an Institute of Physics journal* **23**, 382202 (2011).
22. Chiba, D. *et al.* Electric-field control of magnetic domain-wall velocity in ultrathin cobalt with perpendicular magnetization. *Nat. Commun.* **3**, 888 (2012).
23. Miron, I. M. *et al.* Fast current-induced domain-wall motion controlled by the Rashba effect. *Nat. Mater.* **10**, 419–423 (2011).
24. Liu, L. Q., Lee, O. J., Gudmundsen, T. J., Ralph, D. C. & Buhrman, R. A. Current-Induced Switching of Perpendicularly Magnetized Magnetic Layers Using Spin Torque from the Spin Hall Effect. *Phys. Rev. Lett.* **109**, 096602 (2012).
25. Ryu, K. S., Thomas, L., Yang, S. H. & Parkin, S. Chiral spin torque at magnetic domain walls. *Nat. Nanotechnol.* **8**, 527–533 (2013).
26. Yang, S. H., Ryu, K. S. & Parkin, S. Domain-wall velocities of up to 750 m s<sup>-1</sup> driven by exchange-coupling torque in synthetic antiferromagnets. *Nat. Nanotechnol.* **10**, 221–226 (2015).
27. He, J., Li, Z. & Zhang, S. Current-driven domain-wall depinning. *J. Appl. Phys.* **98**, 016108 (2005).
28. Atkinson, D., Eastwood, D. S. & Bogart, L. K. Controlling domain wall pinning in planar nanowires by selecting domain wall type and its application in a memory concept. *Appl. Phys. Lett.* **92**, 022510 (2008).
29. Himeno, A., Kondo, K., Tanigawa, H., Kasai, S. & Ono, T. Domain wall ratchet effect in a magnetic wire with asymmetric notches. *J. Appl. Phys.* **103**, 07E703 (2008).
30. Hayashi, M. *et al.* Dependence of current and field driven depinning of domain walls on their structure and chirality in permalloy nanowires. *Phys. Rev. Lett.* **97**, 207205 (2006).
31. Huang, S. H. & Lai, C. H. Domain-wall depinning by controlling its configuration at notch. *Appl. Phys. Lett.* **95**, 032505 (2009).
32. Polenciu, I. *et al.* Domain wall pinning for racetrack memory using exchange bias. *Appl. Phys. Lett.* **105**, 162406 (2014).
33. King, J. A. *et al.* Local control of magnetic damping in ferromagnetic/non-magnetic bilayers by interfacial intermixing induced by focused ion-beam irradiation. *Appl. Phys. Lett.* **104**, 242410 (2014).
34. Burn, D. M. & Atkinson, D. Control of domain wall pinning by localised focused Ga<sup>+</sup> ion irradiation on Au capped NiFe nanowires. *J. Appl. Phys.* **116**, 163901 (2014).
35. Rantschler, J. O. *et al.* Effect of 3d, 4d, and 5d transition metal doping on damping in permalloy thin films. *J. Appl. Phys.* **101**, 033911 (2007).
36. Faulkner, C. C., Atkinson, D., Allwood, D. A. & Cowburn, R. P. Rapid tuning of Ni81Fe19/Au bilayer magnetic properties by focused ion beam intermixing. *J. Magn. Magn. Mater.* **319**, 9–12 (2007).
37. Benitez, M. J. *et al.* Engineering Magnetic Domain-Wall Structure in Permalloy Nanowires. *Phys. Rev. Applied* **3**, 034008 (2015).
38. Mizukami, S., Ando, Y. & Miyazaki, T. Ferromagnetic resonance linewidth for NM/80NiFe/NM films (NM = Cu, Ta, Pd and Pt). *J. Magn. Magn. Mater.* **226**, 1640–1642 (2001).
39. He, S. *et al.* A versatile rotary-stage high frequency probe station for studying magnetic films and devices. *Rev. Sci. Instrum.* **87**, 074704 (2016).
40. He, S. K. & Panagopoulos, C. A broadband ferromagnetic resonance dipper probe for magnetic damping measurements from 4.2 K to 300 K. *Rev. Sci. Instrum.* **87**, 043110 (2016).
41. Yin, Y. L. *et al.* Tunable permalloy-based films for magnonic devices. *Phys. Rev. B* **92**, 024427 (2015).
42. Fukami, S., Anekawa, T., Zhang, C. & Ohno, H. A spin-orbit torque switching scheme with collinear magnetic easy axis and current configuration. *Nat. Nanotechnol.* **11**, 621–625 (2016).
43. Jin, L. C., Zhang, H. W., Tang, X. L. & Zhong, Z. Y. Tuning the spin pumping characteristics in Ni81Fe19/CuNx bilayer films. *J. Appl. Phys.* **113**, 17C503 (2013).
44. Ruiz-Calaforra, A. *et al.* The role of the non-magnetic material in spin pumping and magnetization dynamics in NiFe and CoFeB multilayer systems. *J. Appl. Phys.* **117**, 163901 (2015).
45. Ganguly, A. *et al.* Tunable Magnetization Dynamics in Interfacially Modified Ni81Fe19/Pt Bilayer Thin Film Microstructures. *Sci. Rep.* **5**, 17596 (2015).
46. Tserkovnyak, Y., Brataas, A. & Bauer, G. E. W. Spin pumping and magnetization dynamics in metallic multilayers. *Phys. Rev. B* **66**, 224403 (2002).
47. Balavijayalakshmi, J., Suriyanarayanan, N. & Jayaprakash, R. Role of copper on structural, magnetic and dielectric properties of nickel ferrite nano particles. *J. Magn. Magn. Mater.* **385**, 302–307 (2015).
48. Masrour, R., Hamedoun, M., Benyoussef, A. & Hlil, E. K. Magnetic properties of mixed Ni-Cu ferrites calculated using mean field approach. *J. Magn. Magn. Mater.* **363**, 1–5 (2014).
49. Pashchenko, V. P., Shemyakov, A. A. & Loiko, A. D. Structure and properties of copper-doped nickel zinc ferrites. *Inorg. Mater.* **34**, 506–508 (1998).
50. Piramanayagam, S. N. Perpendicular recording media for hard disk drives. *J. Appl. Phys.* **102**, 011301 (2007).

## Acknowledgements

We gratefully acknowledge Nanyang Technological University Start-Up Grant and MOE AcRF-Tier 1 grant RG163/15 for the funding of this research and partial support of NTU-JSPS research grant.

## Author Contributions

T.L.Jin and M.Ranjbar designed the experiment. T.L. Jin fabricated the samples and carried out the experimental measurements. T.L. Jin, M.Ranjbar, S.K.He, W.C.Law and S.N. Piramanayagam analyzed the data. T.L.Jin, M.Ranjbar and S.N. Piramanayagam wrote the manuscript. X.X.Liu carried out some experimental measurements

on NiFe wires. The project was conceived and supervised by S.N. Piramanayagam. All authors discussed the results and commented on the manuscript.

### Additional Information

**Competing Interests:** The authors declare that they have no competing interests.

**Publisher's note:** Springer Nature remains neutral with regard to jurisdictional claims in published maps and institutional affiliations.



**Open Access** This article is licensed under a Creative Commons Attribution 4.0 International License, which permits use, sharing, adaptation, distribution and reproduction in any medium or format, as long as you give appropriate credit to the original author(s) and the source, provide a link to the Creative Commons license, and indicate if changes were made. The images or other third party material in this article are included in the article's Creative Commons license, unless indicated otherwise in a credit line to the material. If material is not included in the article's Creative Commons license and your intended use is not permitted by statutory regulation or exceeds the permitted use, you will need to obtain permission directly from the copyright holder. To view a copy of this license, visit <http://creativecommons.org/licenses/by/4.0/>.

© The Author(s) 2017